Available online at www.sciencedirect.com
ScienceDirect
Ceramics International 37 (2011) 3499–3507
CERAMICS INTERNATIONAL
www.elsevier.com/locate/ceramint

Characterization of $SrWO_4$–PVA and $SrWO_4$ spiders' webs synthesized by electrospinning

Surangkana Wannapop [a], Titipun Thongtem [b,c,*], Somchai Thongtem [a,c]

[a] Department of Physics and Materials Science, Faculty of Science, Chiang Mai University, Chiang Mai 50200, Thailand
[b] Department of Chemistry, Faculty of Science, Chiang Mai University, Chiang Mai 50200, Thailand
[c] Materials Science Research Center, Faculty of Science, Chiang Mai University, Chiang Mai 50200, Thailand

Received 30 March 2011; received in revised form 31 May 2011; accepted 6 June 2011
Available online 12 June 2011

Abstract

Mixtures of strontium acetate, ammonium metatungstate hydrate, and different contents of poly (vinyl alcohol) (PVA, 125,000 MW) were electrospun by a +15 kV direct voltage to synthesize $SrWO_4$–PVA spiders' webs. The spider's web, synthesized from the solution containing 1.3 g PVA, was further calcined in air at 300–600 °C for 3 h. The $SrWO_4$–PVA spider's web was analyzed by thermogravimetric analyzer (TGA) to specify the evaporation and decomposition of PVA and volatile components. In addition, the $SrWO_4$–PVA and $SrWO_4$ spiders' webs were characterized by X-ray diffractometer (XRD), selected area electron diffraction (SAED), scanning and transmission electron microscopes (SEM, TEM), and ultraviolet (UV)–visible and photoluminescence (PL) spectrometers, including the vibration modes by Fourier transform infrared (FTIR) and Raman spectrometers. A possible formation mechanism of $SrWO_4$–PVA and $SrWO_4$ spiders' webs was also proposed according to the experimental results.

Keywords: A. Electrospinning; B. Electron microscopy; C. Optical properties; E. Sensors

1. Introduction

Strontium tungstate, one of scheelite-type tetragonal metal tungstates, is very interesting for a variety of applications, such as photoluminescence, light emitting diodes (LEDs), solid state Raman lasers, optical fibers, scintillating materials, humidity sensors, and catalysts [1–5]. It belongs to $I4_1/a$ space group with two formula units per primitive cell. Each of W atoms is surrounded by four equivalent O atoms composing the $[WO_4]^{2-}$ tetrahedral configuration, and each divalent strontium atom shares corners with eight adjacent O atoms of $[WO_4]^{2-}$ tetrahedrons [3,4]. It is very interesting and attractive phosphor material, due to its structural properties, great potential and promising applications, excellent thermal and hydrolytic stability, strong absorption in the near ultraviolet range, and good mechanical property and Raman gains [2,3,5].

Nanomaterials have very interesting properties, which are different from their bulks. These properties are controlled by uniform shape and narrow size distribution [6,7]. There are a variety of methods used to synthesize metal tungstates, such as high temperature solid state reaction in ambient air [2,3], spray pyrolysis [7], co-precipitation [4], sonochemistry [1,8], and Czochralski method [9].

Basically, there are three components used to synthesize electrospun fibers by the electrospinning process: a direct current (d.c.) power supply, a long hollow needle, and an electrical conducting screen. During electrospinning, a drop of polymeric solution at the tip of the hollow needle is charged by a positive direct high voltage. The mutual positive charge repulsion on the polymeric droplet is created. When the applied d.c. voltage is increased, the liquid droplet is stretched to be a conical shape, known as Taylor cone. Upon further increasing the d.c. voltage until it is sufficiently high, the repulsive force overcomes the surface tension of the polymeric liquid, and the jet of liquid is ejected out of the Taylor cone. Meanwhile, the

? Corresponding author at: Department of Chemistry, Faculty of Science, Chiang Mai University, Chiang Mai 50200, Thailand. Tel.: +66 (0) 53 943344; fax: +66 (0) 53 892277.
E-mail addresses: ttpthongtem@yahoo.com, ttpthongtem@hotmail.com (T. Thongtem).

0272-8842/$36.00
doi:10.1016/j.ceramint.2011.06.005

liquid jet evaporates and solidifies, leaving behind the polymeric fibers deposited on the ground-conducting screen [10].

There are several parameters that have the influence on the electrospun fibers: (a) variable parameters of the electrospinning equipment (applied voltage at the needle tip as well as electric field inside the fiber, pressure used to push the liquid out of the hollow needle, and distance between the needle tip and the ground conducting screen), (b) solution properties (viscosity, surface tension, elasticity, and conductivity), and (c) ambient parameters (temperature, humidity, and wind blow). These can play the role in the morphologies of the electrospun fiber, like fibrous diameter, number of the beads including their shape and size, and defects (pores) on the fiber [11]. Inclination (vertical or horizontal) of the hollow needle has the influence on the fiber as well.

$SrWO_4$–PVA spiders' webs are very novel and promising products for a variety of applications. They are able to be synthesized by a high d.c. voltage electrospinning process. To the best of our knowledge, no $SrWO_4$–PVA spiders' webs have ever been synthesized by this process. In the present research, the mixture of inorganic and polymeric materials were used to synthesize the inorganic material-polymer electrospun fibrous webs, which would transformed into nanofibrous inorganic material webs by subsequent calcination at high temperatures. Moreover, the success in synthesizing the solid nanofibrous webs may lead to a new process for industrial scale production.

2. Experiment

In the present research, 4.5 mmol strontium acetate [$Sr(CH_3COO)_2$], 4.5 mmol ammonium metatungstate hydrate ($H_{26}N_6O_{40}W_{12}{\cdot}xH_2O$), and different contents of poly (vinyl alcohol) (PVA, 125,000 MW) were separately dissolved in 10 ml deionized water each, mixed, and vigorously stirred at 80 °C for 30 min. These mixtures were encoded as M10, M11, M12, and M13 for using 1.0, 1.1, 1.2, and 1.3 g PVA, respectively. Each of them was electrospun by a horizontal syringe needle biased with +15 kV from a d.c. power supply, to synthesize $SrWO_4$–PVA spiders' webs on a grounded vertical flat aluminum foil. The $SrWO_4$–PVA spider's web synthesized from the M13 mixture was selected to be calcined in air at 300 °C, 400 °C, 500 °C and 600 °C for 3 h, to synthesize $SrWO_4$ nanoparticles joined together as a spider's web. These products were characterized using thermogravimetric analyzer (TGA, Shimadzu TGA-50 analyzer, Japan) using a heating rate of 5 °C/min; X-ray diffractometer (XRD, SIEMENS D500, Germany) operating at 20 kV, 15 mA, and using Cu-Kα line, in combination with the database of the Joint Committee on Powder Diffraction Standards (JCPDS) [12]; scanning electron microscope (SEM, JEOL JSM-6335F, Japan) operating at 15 kV; transmission electron microscope (TEM, JEOL JEM-2010, Japan), high resolution transmission electron microscope (HRTEM) and selected area electron diffractometer (SAED) operating at 200 kV; Fourier transform infrared spectrometer (FTIR, Bruker Tensor 27, Germany) with KBr as a diluting agent and operated in the range of 4000–400 cm^{-1}; Raman spectrometer (T64000 HORIBA Jobin Yvon, U.S.A.) using a 50 mW and 514.5 nm wavelength Ar green laser; UV–vis spectrometer (Lambda 25 PerkinElmer, U.S.A.) using a UV lamp with the resolution of 1 nm; and photoluminescence (PL) spectrometer (LS 50B PerkinElmer, U.S.A.) using a 245 nm excitation wavelength at room temperature.

3. Results and discussion

3.1. TGA

Fig. 1 compares TGA curve of the M13 spider's web to that of PVA. The weight loss of pure PVA exhibited the evaporation and degradation processes for three steps over the temperature range of 32–494 °C. First, the weight loss of 9.5% was caused by the evaporation of loosely bound water at 32–194 °C. Second, the large amount of weight loss of 79.7% was predominantly due to the decomposition of PVA structure at 194–415 °C. Third, the 9.3% weight loss was by the breaking of PVA main chains at 415–494 °C. The weight loss tended to terminate upon further heating at above 494 °C [13].

Consider TGA curve of the M13 spider's web, the weight losses were divided into three different steps. The first weight loss at 32–218 °C was 15.8%, and associated with water evaporation. The second weight loss of 25.5% at 218–405 °C was caused by the decomposition of PVA. The final weight loss of 18.2% at 405–520 °C seemed to be the oxidation and decomposition of the PVA main chains. These last two steps were attributed to the loss of PVA and organic compound blended in the fibers. At a temperature above 520 °C, there was no significant change in their weight.

3.2. XRD

Fig. 2 shows XRD patterns of $SrWO_4$–PVA spider's web, synthesized from the M13 solution, after calcination at 300 °C, 400 °C, 500 °C and 600 °C for 3 h. Comparing with the JCPDS database no. 08-0490 [12], they were specified as the crystalline

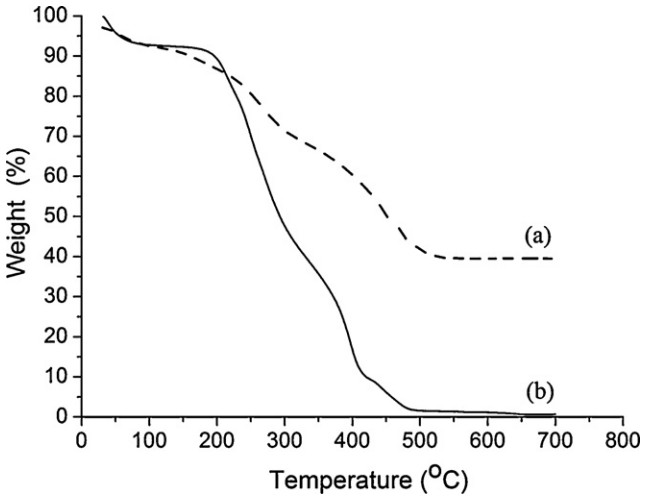

Fig. 1. TGA curves of (a) a spider's web synthesized from the M13 solution, and (b) PVA.

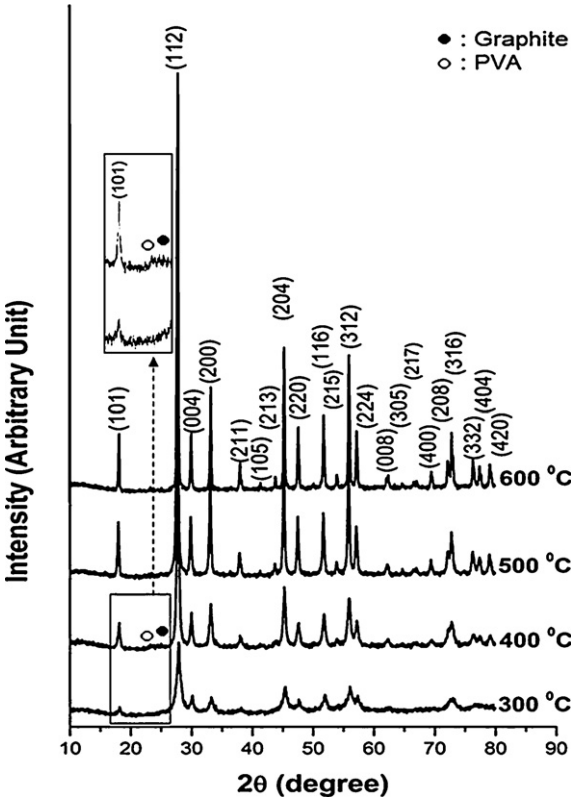

Fig. 2. XRD patterns of $SrWO_4$–PVA spider's web, synthesized from the M13 solution, after calcination at 300 °C, 400 °C, 500 °C and 600 °C for 3 h.

phase of tetragonal system ($a = b = 5.4168$ Å, $c = 11.9510$ Å, and $\alpha = \beta = \gamma = 90°$) of $SrWO_4$ structure. At 300 °C calcination, the peaks of $SrWO_4$ were quite broad. This product contained very small contents of residual PVA at $2\theta = 22.5°$ [14], and graphite at $2\theta = 26.3°$ of JCPDS database no. 01-0640 [12] caused by the decomposition of PVA. The product has the color of light grey, due to some graphite residue. Upon calcination at 400 °C, both residual PVA and graphite were reduced, due to the evaporation of PVA and oxidation of graphite to be its oxides in gaseous form. Until at 500 °C and 600 °C calcination, they were no longer detected by the XRD. In addition, the XRD peaks became narrower and sharper, implying the improvement of products' crystalline degree and purity. At 600 °C calcination, the product was the best pure white crystalline $SrWO_4$.

Their average lattice parameters, calculated from the plane-spacing equation for tetragonal structure and Bragg's law for diffraction [15], were $a = b = 5.388$ Å, and $c = 11.898$ Å—very close to their corresponding standard values [12]. For scheelite structured $SrWO_4$, each Sr divalent ion was surrounded by eight O ions with each W ion in the tetrahedrons of O ions [4,16].

3.3. FTIR

The FTIR spectra (Fig. 3) were provided further insight into the structure of PVA, and $SrWO_4$–PVA spider's web synthesized from the M13 solution, before and after calcination at 300 °C, 400 °C, 500 °C and 600 °C for 3 h. Consider the PVA spectrum, a broad strong O–H stretching mode of alcohol and residual water was detected at 3600–3200 cm^{-1}. It was the stretching of hydroxyl groups with strong hydrogen bonding of

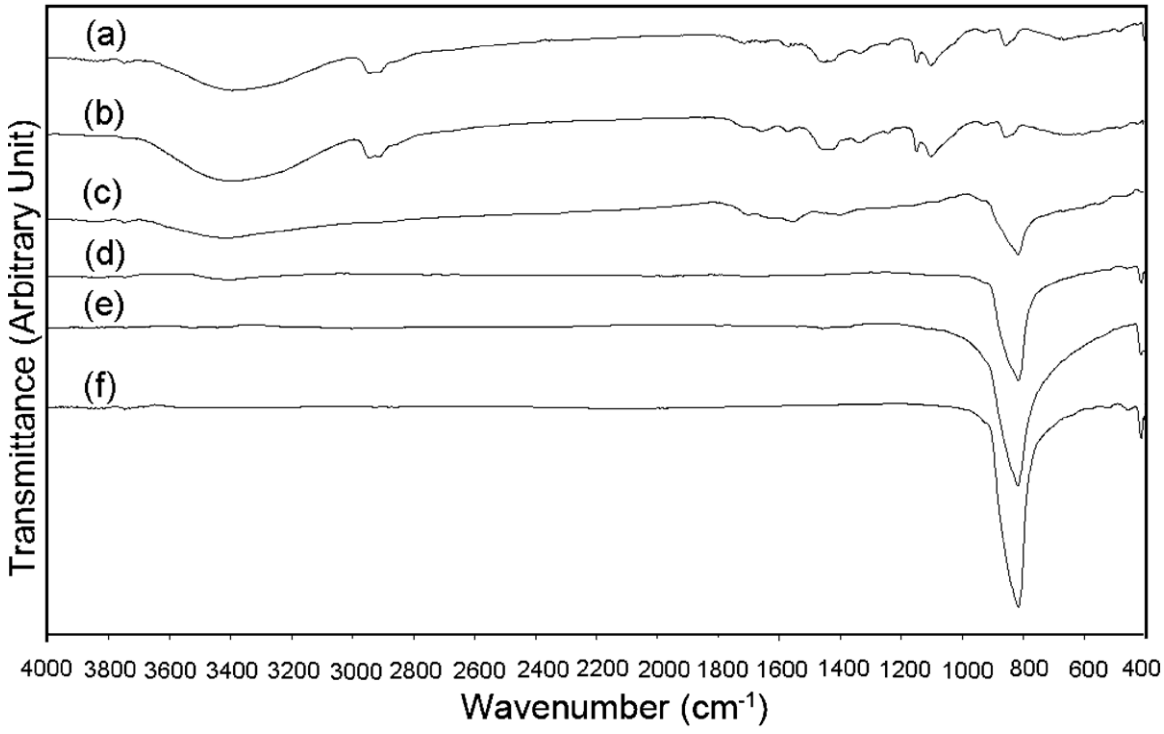

Fig. 3. FTIR spectra of (a) PVA, and (b)–(f) $SrWO_4$–PVA spider's web, synthesized from the M13 solution, before and after calcination at 300 °C, 400 °C, 500 °C and 600 °C for 3 h, respectively.

intra- and inter-types. Two strong vibration modes at 2945 and 2909 cm^{-1} corresponded to the asymmetric and symmetric C–H stretching of alkyl groups, respectively. The C=O stretching mode at 1656 cm^{-1} was caused by the carbonyl functional groups of the acetate remaining in PVA by the hydrolysis of polyvinyl acetate and oxidation process during manufacturing. The C=C stretching mode at 1566 cm^{-1} was caused by cross-linking of the PVA during heating. The presence of C=O and/or C=C stretching modes implied that PVA molecules have the same resonant structures: alkene ↔ alkane, and C=O ↔ C–O^-, or the presence of hydrogen bonds with oxygen of C=O groups. The 1439 cm^{-1} was specified as the CH_2 bending mode, the 1342 cm^{-1} as the C–CH_3 deformation vibration, and the 1241 cm^{-1} as the CH_2 wagging mode. The C–C and C–O–C stretching vibrations, recognized as the crystallization sensitive modes, were detected at 1147 cm^{-1}. The vibration at 1096 cm^{-1} was specified as the C–O stretching, and at 851 cm^{-1} as the C–C stretching [17]. Once, the as-synthesized $SrWO_4$-PVA spider's web was characterized by FTIR, additional modes of $SrWO_4$ were detected. For T_d-symmetry, vibration frequencies of $[WO_4]^{2-}$ tetrahedrons were $\nu_1(A_1)$, $\nu_2(E)$, $\nu_3(F_2)$ and $\nu_4(F_2)$ [18]. In lattice space, the site symmetries became S_4. The correlation of the two point groups ($T_d \rightarrow S_4$) is the following: $A_1 \rightarrow A$, $E \rightarrow A + B$ and $F_2 \rightarrow B + E$. Only the modes corresponding to ν_2, ν_3 and ν_4 were detected [18]. Main transmittance mode (ν_3) specified as W–O anti-symmetric stretching vibration of $[WO_4]^{2-}$ tetrahedrons in lattice space [18] was detected at 638–1003 cm^{-1}. Sometimes it split into two modes, sometimes it did not [18–20]. In the present research, they appeared as the strong broad band. The ν_4 split into two modes at the wavenumbers of less than 400 cm^{-1} [18]. When the $SrWO_4$–PVA spider's web was calcined in air at 300–600 °C for 3 h, the PVA and residual water began to evaporate and decompose. Additional weak peaks of W–O vibrations for 300 °C, 400 °C, 500 °C, and 600 °C were also detected at 410 cm^{-1}, specified as ν_2 bending modes [18,21]. At higher temperatures, the FTIR intensities were strengthened. The evaporation rates of PVA and water became faster, and their residues were lessened. Until at 600 °C calcination, the vibrations of PVA and water were no longer detected. The ν_3 anti-symmetric stretching and ν_2 bending modes became the strongest, and the product was really $SrWO_4$ electrospun nanofibrous web.

3.4. Raman analysis

The Raman vibrations of $SrWO_4$ were divided into two groups, the internal and external [22]. The internal mode was the W–O vibration within the $[WO_4]^{2-}$ tetrahedral units with immobile mass centers. The external or lattice phonon mode corresponded to the vibration of Sr^{2+} cations relative to the rigid $[WO_4]^{2-}$ tetrahedral units. In free space, $[WO_4]^{2-}$ tetrahedrons have T_d-symmetry [22,23]. Their vibrations were specified as four internal modes of $\nu_1(A_1)$, $\nu_2(E)$, $\nu_3(F_2)$ and $\nu_4(F_2)$, one free rotation of $\nu_{f.r.}(F_1)$, and one translation (F_2) [22]. In lattice space, they have S_4-symmetry. All degenerative vibrations were split [22,23] due to the crystal field effect and Davydov splitting [22]. According to group-theory calculation, there are 26 different modes for tetragonal scheelite primitive cell with zero wavevector ($\vec{k} = \vec{0}$): three for A_g and B_u, and five for A_u, B_g, E_g and E_u each. All modes of A_g, B_g and E_g were Raman-active. Four of five A_u and E_u modes were IR-active, and their remains were acoustic vibrations. Three vibrations of B_u were silent modes [22,24]. In the present research, six different modes of $\nu_1(A_g)$, $\nu_3(B_g)$, $\nu_3(E_g)$, $\nu_4(B_g)$, $\nu_2(A_g)$ and free rotation were detected on the Raman spectrum (Fig. 4) at 912, 831, 791, 373, 334 and 187 cm^{-1}—in accordance with those of the previous reports [22,23]. This spectrum provided the evidence of scheelite structure of $SrWO_4$ [22,23] spider's web. Comparing to Ar laser (λ = 514.5 nm), a great deal of energy was lost during the inelastic scattering process.

3.5. SEM, TEM, HRTEM, and SAED

The $SrWO_4$–PVA spiders' webs synthesized from the solutions containing different contents of PVA are shown in Fig. 5a–d. The spiders' webs of the M10, M11, M12, and M13 solutions, respective containing 1.0, 1.1, 1.2, and 1.3 g PVA, were composed of fibers woven like spiders' webs. Some beads were also detected; especially, those synthesized from the mixtures of less than 1.3 g PVA. The number of beads was lessened in sequence with the increase of the PVA masses, and was no longer detected for 1.3 g PVA (M13) solution. The content of PVA can also play the role in the viscosity of the mixtures, which influenced the stability of the solution jets. For 1.3 g PVA, it was exactly right to eject the inorganic material-polymeric solution through the syringe out of the hollow needle, and the web was composed of the bead-free fibers. These implied that the fibers and beads were influenced by the stability of the jet of inorganic material-polymeric solutions, and PVA contents [11,25]. The M13 spider's web was then selected for further studies.

When the $SrWO_4$–PVA spider's web was calcined at 300–600 °C for 3 h (Figs. 5e–h and 6a, b, e and f), the fibers became thinner, due to the evaporation and decomposition of PVA and

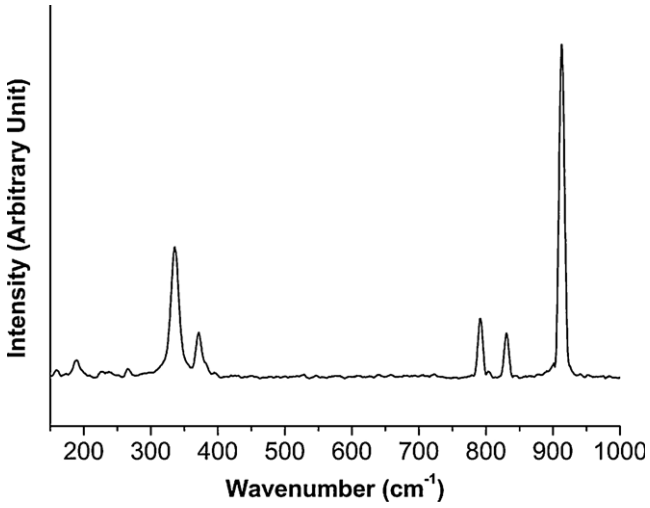

Fig. 4. Raman spectrum of $SrWO_4$ spider's web, synthesized from the M13 solution.

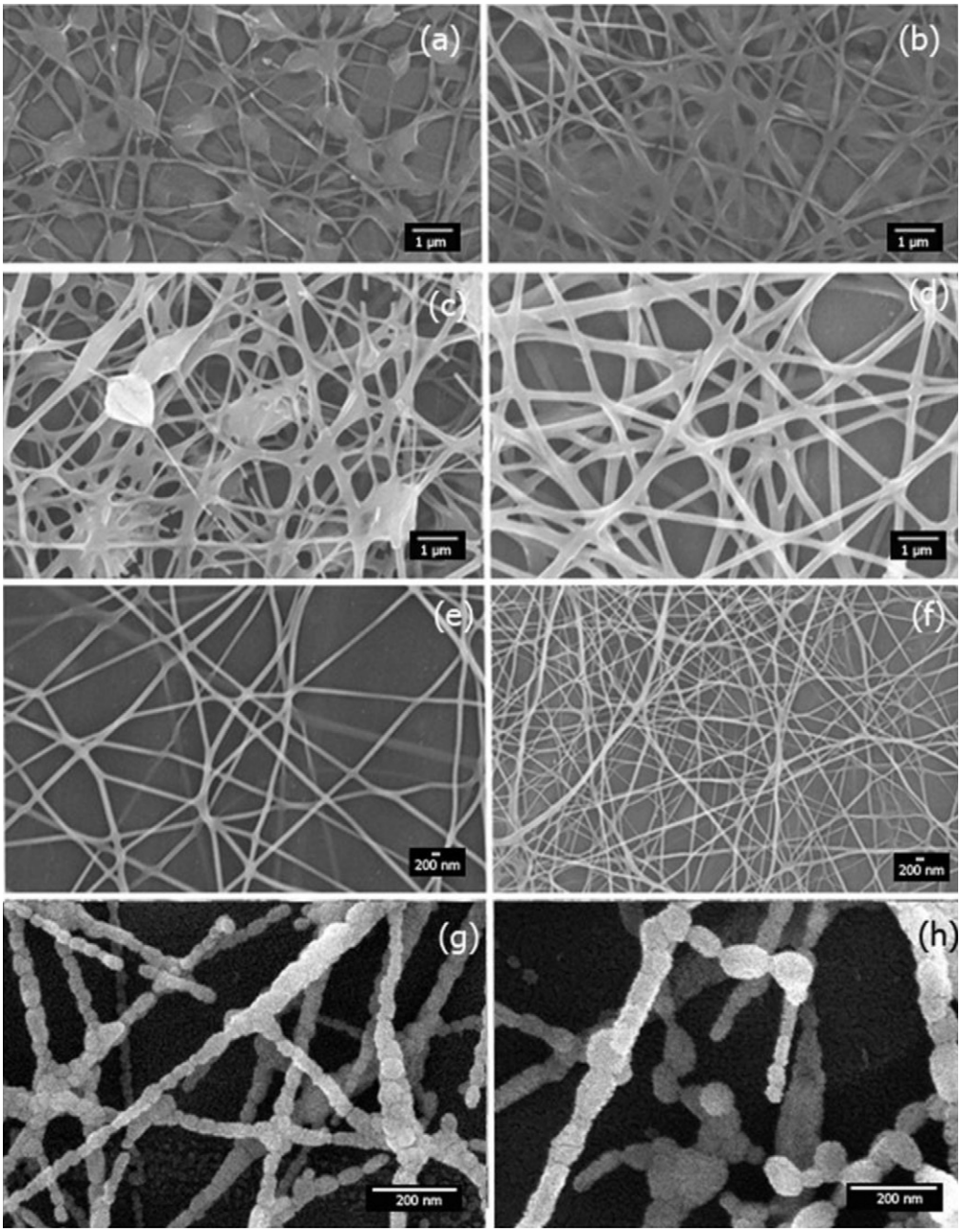

Fig. 5. SEM images of (a)–(d) $SrWO_4$–PVA spiders' webs synthesized from the M10, M11, M12, and M13 solutions, and (e)–(h) $SrWO_4$–PVA spider's web synthesized from the M13 solution after calcination at 300 °C, 400 °C, 500 °C, and 600 °C for 3 h, respectively.

volatile components. $SrWO_4$ nuclei also grew to form larger nanoparticles. Upon increasing the calcination temperatures, the evaporation and decomposition rates of PVA, as well as the growth rate of $SrWO_4$ nanoparticles, were increased. It was more than likely that PVA did not remain in the products with 500 °C and 600 °C calcination. These products were composed of nanoparticles with different sizes and orientations joined together like a spider's web. For close examination on a nanoparticle calcined at 500 °C, a number of parallel crystallographic planes were detected by HRTEM (Fig. 6b). They were specified as the (1 0 1) plane of tetragonal structured $SrWO_4$, implying that the nanoparticle was really a single crystal. SAED patterns were interpreted [26], and specified as the (1 0 1), (1 1 2) and (0 1 1) planes (Fig. 6c) with electron beam in the $[\bar{1}\,\bar{1}\,1]$ direction, and the (2 0 0), (2 2 0) and (0 2 0) planes (Fig. 6g) with electron beam in the [0 0 1] direction for the nanoparticles of 500 °C and 600 °C calcination, respectively. They corresponded to the JCPDS database for tetragonal structured $SrWO_4$ [12]–in good accordance with the above XRD analysis. Diffraction patterns of these products (Fig. 6d and h) were also simulated [27] using the corresponding electron beams. They are in systematic and symmetric order, with the a*, b* and c* reciprocal lattice vectors for both patterns in the [1 0 0], [0 1 0], and [0 0 1] directions. For one crystal structure, the corresponding reciprocal lattice vectors were the same although the electron beams were different. Comparing

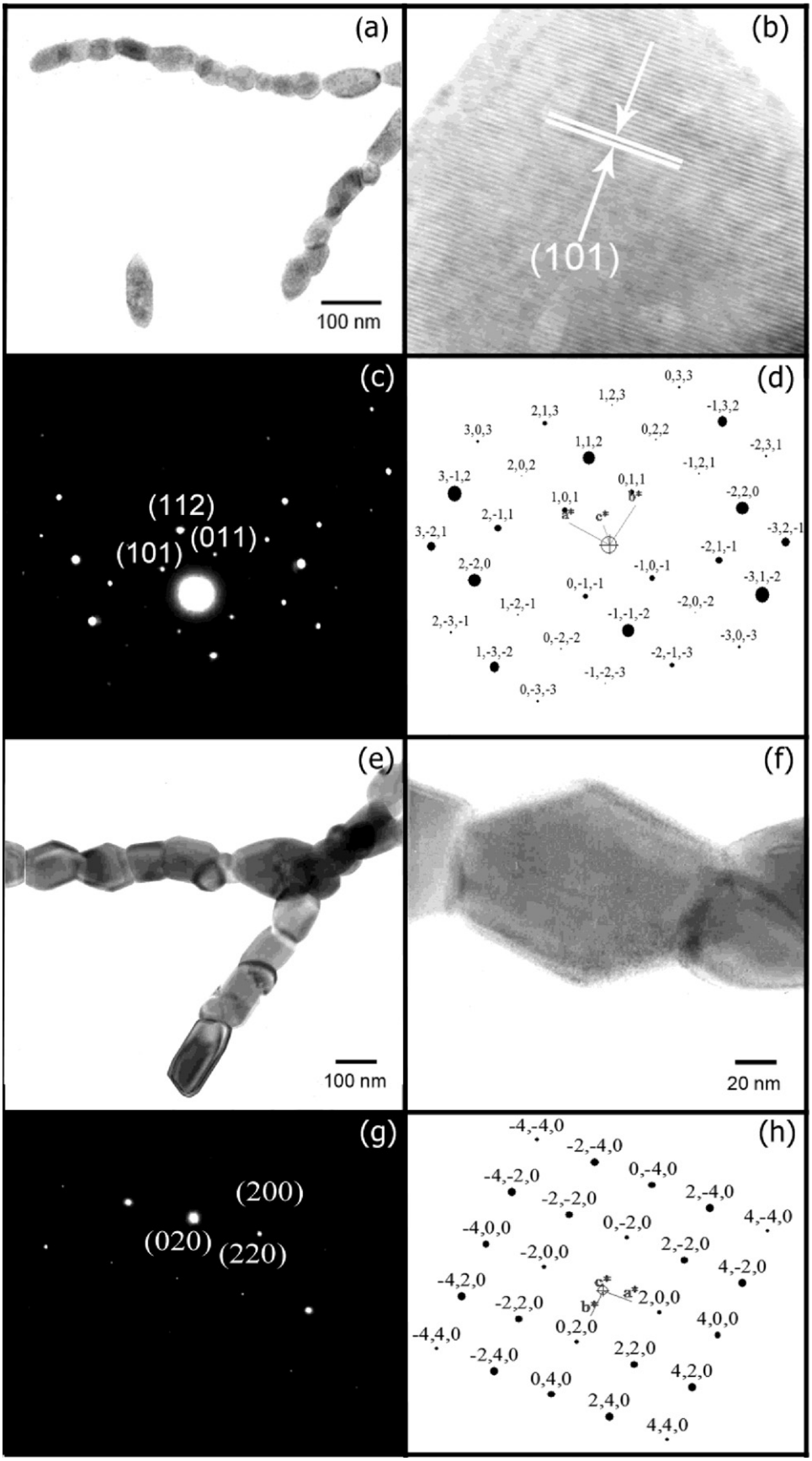

Fig. 6. TEM and HRTEM images, and SAED and simulated patterns of $SrWO_4$–PVA spider's web, synthesized from the M13 solution, after calcination at (a)–(d) 500 °C, and (e)–(h) 600 °C for 3 h.

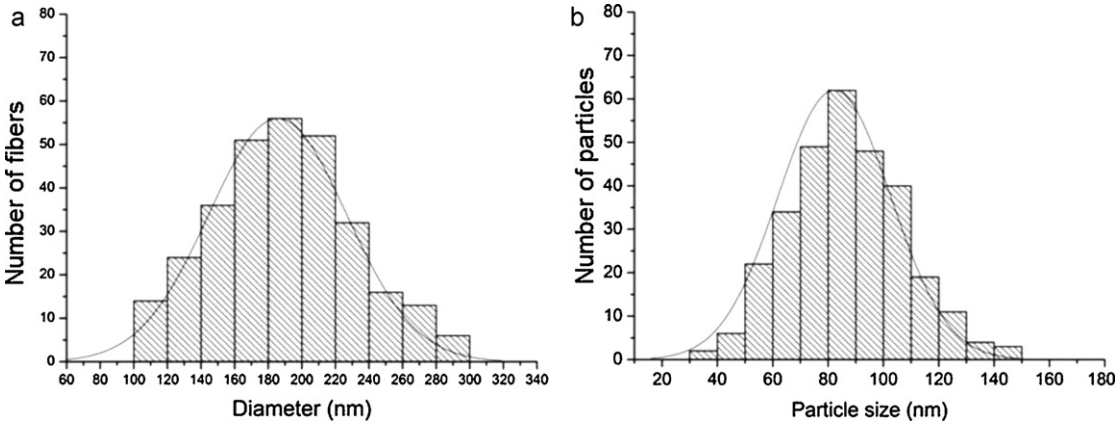

Fig. 7. (a) and (b) Distributions of fibrous diameters and particle sizes of the $SrWO_4$–PVA spider's web, synthesized from the M13 solution, before and after calcination at 600 °C for 3 h, respectively.

between the corresponding interpreted and simulated patterns, they are in good accordance.

3.6. Distributions of fibers and particles

Distributions of fibrous diameters and particle sizes of the spider's web, synthesized from the M13 solution, before and after calcination at 600 °C for 3 h are shown in Fig. 7. These fibrous diameters and particle sizes were started to be counted and arranged from the smallest to the largest values. Their distributions fitted very well with normal curves over the ranges of 60–320 nm with the average of 185.6 nm diameter, and 20–150 nm with the average of 82.3 nm particle size.

3.7. Formation mechanism

During electrospinning, electric field from a +15 d.c. kV voltage generated heat through the mixture of $Sr(CH_3COO)_2$, $H_{26}N_6O_{40}W_{12}{\cdot}xH_2O$, and PVA. Sr^{2+} cations (electron pair acceptors—Lewis acid) chemically combined with $[WO_4]^{2-}$ anions (electron pair donors—Lewis base). The chemical reaction between these two species ($Sr^{2+} \leftarrow :WO_4^{2-}$) proceeded to form covalent bonds. The lowest molecular orbital energy of Lewis acid interacted with the highest molecular orbital energy of Lewis base. $SrWO_4$ molecules were finally synthesized [4,28], and nucleated to form nuclei, blended in the PVA fibrous template. Due to the electrospinning, the products were in the shape of spiders' webs. Upon calcination at high temperatures, $SrWO_4$ nuclei grew to form larger nanoparticles. Their growth rates were increased with the increasing in the calcination temperatures. At 600 °C calcination, the product was composed of a number of the biggest $SrWO_4$ nanoparticles joined together like nanofibers, woven in the shape of a spider's web.

3.8. UV–vis absorption

Fig. 8 shows the $(\alpha h\nu)^2$ vs $h\nu$ curve of the $SrWO_4$ spider's web. By using Wood and Tauc equation [4,16,28–30] below.

$$\alpha h\nu = \left(h\nu - E_g\right)^n \quad (1)$$

where α is the absorbance, h the Planck constant, ν the photon frequency, E_g the energy gap, and n the pure numbers associated with the different types of electronic transitions. For n = 1/2, 2, 3/2 and 3, the transitions are the direct allowed, indirect allowed, direct forbidden, and indirect forbidden, respectively. It should be noted that the absorption was controlled by two photon energy ($h\nu$) ranges—the high and low energies. When the photon energy was greater than the energy band gap, absorption was linearly increased with the increasing of photon energy. The steep inclination of the linear portion of the curve was caused by the UV absorption for charged transition from the topmost occupied state of valence band to the bottommost unoccupied state of the conduction band. For the photon energy with less than the energy band gap, the absorption curve became different from linearity, due to the UV absorption for charged transition relating to different defects. The direct energy gap (E_g) was determined by extrapolating the linear portion of the curve to the zero absorbance. In the present research, $SrWO_4$ with scheelite-type tetragonal structure presented the direct allowed electronic transition [4,28,30], with

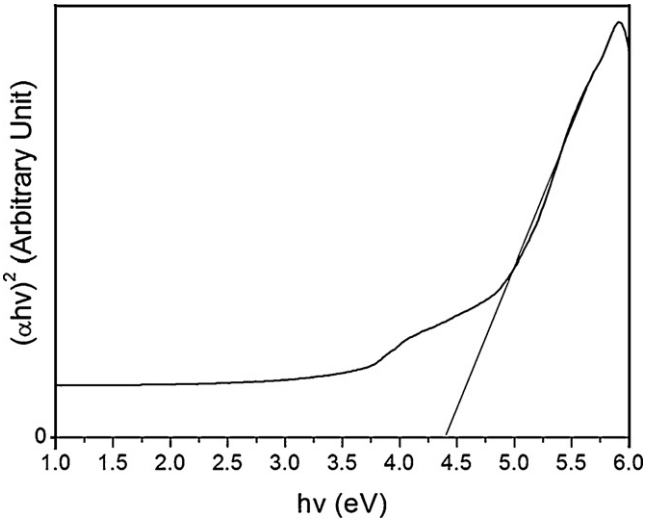

Fig. 8. The $(\alpha h\nu)^2$ versus $h\nu$ plot of the $SrWO_4$ spider's web, synthesized from the M13 solution.

the energy gap of 4.47 eV—in good accordance with the previous reports [16]. In fact, energy gap is controlled by several factors such as the electronegativity of transition metal ions, connectivity of the polyhedrons, deviation in the O–W–O bonds, distortion of the $[WO_4]^{2-}$ tetrahedrons, growth mechanism, and degree of structural order–disorder in the lattice [16,28].

3.9. Photoluminescence

PL spectra of $SrWO_4$–PVA spider's web, synthesized from the M13 solution, after calcination at 300 °C, 400 °C, 500 °C and 600 °C for 3 h (Fig. 9) show the intrinsic peaks with their surrounding shoulders. The intrinsic peaks were due to the $^1T_2 \rightarrow {}^1A_1$ transition of electrons within $[WO_4]^{2-}$ anions [31,32], which were treated as excitons. The shoulders were caused by some defects and/or impurities, and interpreted as extrinsic transition. Generally, PL intensity is controlled by the number of charged transition. In the present research, the emission peaks were in the spectral region at 439–441 nm—having the potential applications for photonic sensors and devices. Starting from 300 °C to 600 °C calcination, PL intensities were 74, 89, 98, and 100%, respectively. They were increased with the increase in the calcination temperatures, and became the highest at 600 °C calcination.

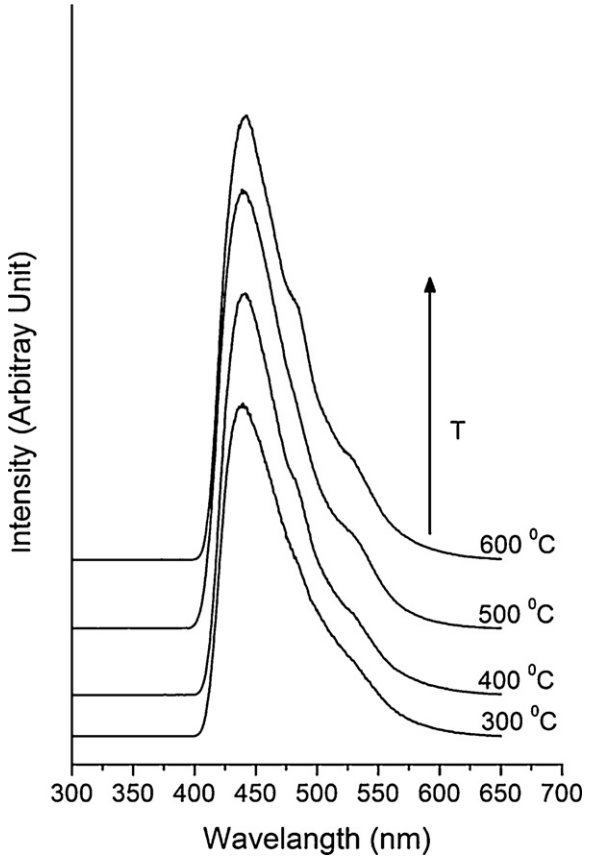

Fig. 9. PL spectra of $SrWO_4$–PVA spider's web, synthesized from the M13 solution, after calcination at 300 °C, 400 °C, 500 °C and 600 °C for 3 h.

4. Conclusions

$SrWO_4$–PVA spiders' webs were synthesized from strontium acetate, ammonium metatungstate hydrate, and different contents of poly (vinyl alcohol) (PVA, 125,000 MW) by the +15 kV direct voltage electrospinning process. In the present research, the $SrWO_4$–PVA spider's web synthesized from the solution containing 1.3 g PVA were further calcined in air at 300 °C, 400 °C, 500 °C and 600 °C for 3 h. At 600 °C calcination, the product was tetragonal scheelite structured $SrWO_4$ nanofibers shaped like a spider's web with the luminescence emission of 439–441 nm, and direct energy gap of 4.47 eV—one of the promising products for a wide variety of applications.

Acknowledgements

We wish to thank the Thailand's Office of the Higher Education Commission for providing financial support through the National Research University (NRU) Project, and the Strategic Scholarships for Frontier Research Network of the Joint Ph.D. Research Program, and the Graduate School of Chiang Mai University for general support.

References

[1] L.D. Feng, X.B. Chen, C.J. Mao, A facile synthesis of $SrWO_4$ nanobelts by the sonochemical method, Mater. Lett. 64 (2010) 2420–2423.
[2] Z.H. Ju, R.P. Wei, J.X. Ma, C.R. Pang, W.S. Liu, A novel orange emissive phosphor $SrWO_4:Sm^{3+}$ for white light-emitting diodes, J. Alloys Compd. 507 (2010) 133–136.
[3] Z. Ju, R. Wei, X. Gao, W. Liu, C. Pang, Red phosphor $SrWO_4:Eu^{3+}$ for potential application in white LED, Opt. Mater. 33 (2011) 909–913.
[4] T. Thongtem, S. Kungwankunakorn, B. Kuntalue, A. Phuruangrat, S. Thongtem, Luminescence and absorbance of highly crystalline $CaMoO_4$, $SrMoO_4$, $CaWO_4$ and $SrWO_4$ nanoparticles synthesized by co-precipitation method at room temperature, J. Alloys Compd. 506 (2010) 475–481.
[5] Y. Duan, F. Yang, H. Zhu, Z. Zhu, C. Huang, Z. You, Y. Wei, G. Zhang, C. Tu, Continuous-wave 560 nm light generated by intracavity $SrWO_4$ Raman and KTP sum-frequency mixing, Opt. Commun. 283 (2010) 5135–5138.
[6] D. Chen, G. Shen, K. Tang, H. Zheng, Y. Qian, Low-temperature synthesis of metal tungstates nanocrystallites in ethylene glycol, Mater. Res. Bull. 38 (2003) 1783–1789.
[7] S. Thongtem, S. Wannapop, T. Thongtem, Characterization of $CoWO_4$ nano-particles produced using the spray pyrolysis, Ceram. Int. 35 (2009) 2087–2091.
[8] T. Thongtem, S. Kaowphong, S. Thongtem, Sonochemical preparation of $PbWO_4$ crystals with different morphologies, Ceram. Int. 35 (2009) 1103–1108.
[9] D. Errandonea, F.J. Manjón, N. Garro, P. Rodríguez-Hernández, S. Radescu, A. Mujica, A. Muñoz, C.Y. Tu, Combined Raman scattering and ab initio investigation of pressure-induced structural phase transitions in the scintillator $ZnWO_4$, Phys. Rev. B 78 (2008) 054116–54121.
[10] J.M. Deitzel, J. Kleinmeyer, D. Harris, N.C. Beck Tan, The effect of processing variables on the morphology of electrospun nanofibers and textiles, Polymer 42 (2001) 261–272.
[11] Z.M. Huang, Y.Z. Zhang, M. Kotaki, S. Ramakrishna, A review on polymer nanofibers by electrospinning and their applications in nanocomposites, Compos. Sci. Technol. 63 (2003) 2223–2253.
[12] Powder Diffract. File, JCPDS-ICDD, 12 Campus Boulevard, Newtown Square, PA 19073-3273, U.S.A. 2001.

[13] E.A. El-hefian, M.M. Nasef, A.H. Yahaya, The preparation and characterization of chitosan/poly (vinyl alcohol) blended films, E-J. Chem. 7 (2010) 1212–1219.
[14] K. Pal, A.K. Banthia, D.K. Majumdar, Preparation and characterization of polyvinyl alcohol–gelatin hydrogel membranes for biomedical applications, AAPS PharmSciTech 8 (2007), doi:10.1208/pt080121, Art. No. 21.
[15] C. Suryanarayana, M.G. Norton, X-ray Diffraction: A Practical Approach, Plenum Press, New York, 1998.
[16] J.C. Sczancoski, L.S. Cavalcante, M.R. Joya, J.W.M. Espinosa, P.S. Pizani, J.A. Varela, E. Longo, Synthesis, growth process and photoluminescence properties of $SrWO_4$ powders, J. Colloids Interface Sci. 330 (2009) 227–236.
[17] Z.I. Ali, F.A. Ali, A.M. Hosam, Effect of electron beam irradiation on the structural properties of PVA/V2O5 xerogel, Spectrochim. Acta Part A 72 (2009) 868–875.
[18] G.M. Clark, W.P. Doyle, Infra-red spectra of anhydrous molybdates and tungstates, Spectrochim. Acta 22 (1966) 1441–1447.
[19] G. Zhang, R. Jia, Q. Wu, Preparation, structural and optical properties of AWO_4 (A = Ca, BaSr) nanofilms, Mater. Sci. Eng. B 128 (2006) 254–259.
[20] F.A. Miller, C.H. Wilkins, Infrared spectra and characteristic frequencies of inorganic ions, Anal. Chem. 24 (1952) 1253–1294.
[21] R.L. Frost, L. Duong, M. Weier, Raman microscopy of selected tungstate minerals, Spectrochim. Acta Part A 60 (2004) 1853–1859.
[22] T.T. Basiev, A.A. Sobol, Y.K. Voronko, P.G. Zverev, Spontaneous Raman spectroscopy of tungstate and molybdate crystals for Raman lasers, Opt. Mater. 15 (2000) 205–216.
[23] S.P.S. Porto, J.F. Scott, Raman spectra of $CaWO_4$, $SrWO_4$, $CaMoO_4$, and $SrMoO_4$, Phys. Rev. 157 (1967) 716–719.
[24] A. Golubović, R. Gajić, Z. Dohčević-Mitrović, S. Nikolić, Nd induced changes in IR spectra of $CaWO_4$ single crystals, J. Alloys Compd. 415 (2006) 16–22.
[25] B. Ding, H.Y. Kim, S.C. Lee, D.R. Lee, K.J. Choi, Preparation and characterization of nanoscaled poly (vinyl alcohol) fibers via electrospinning, Fiber Polym. 3 (2002) 73–79.
[26] K.W. Andrews, D.J. Dyson, S.R. Keown, Interpreting Electron Diffraction Patterns, Plenum Press, New York, 1971.
[27] C. Boudias, D. Monceau, CaRIne Crystallography 3.1, DIVERGENT S.A., Centre de Transfert, 60200 Compiègne, France, 1989–1998.
[28] L.S. Cavalcante, J.C. Sczancoski, R.L. Tranquilin, M.R. Joya, P.S. Pizani, J.A. Varela, E. Longo, $BaMoO_4$ powders processed in domestic microwave-hydrothermal: synthesis, characterization and photoluminescence at room temperature, J. Phys. Chem. Solids 69 (2008) 2674–2680.
[29] J.C. Sczancoski, L.S. Cavalcante, N.L. Marana, R.O. da Silva, R.L. Tranquilin, M.R. Joya, P.S. Pizani, J.A. Varela, J.R. Sambrano, M.S. Li, E. Longo, J. Andrés, Electronic structure and optical properties of $BaMoO_4$ powders, Curr. Appl. Phys. 10 (2010) 614–624.
[30] J.H. Ryu, B.G. Choi, J.W. Yoon, K.B. Shim, K. Machi, K. Hamada, Synthesis of $CaMoO_4$ nanoparticles by pulsed laser ablation in deionized water and optical properties, J. Lumin. 124 (2007) 67–70.
[31] A. Phuruangrat, T. Thongtem, S. Thongtem, Synthesis of lead molybdate and lead tungstate via microwave irradiation method, J. Cryst. Growth 311 (2009) 4076–4081.
[32] A. Phuruangrat, T. Thongtem, S. Thongtem, Preparation, characterization and photoluminescence of nanocrystalline calcium molybdate, J. Alloys Compd. 481 (2009) 568–572.